


Quantum Wire Coupled to Light

Victor Bradley,^{1,*} Kamal Sharma¹,¹ Mohammad Hafezi,^{2,3} and Wade DeGottardi¹

¹Department of Physics and Astronomy, Texas Tech University, Lubbock, Texas 79409, USA

²NIST/University of Maryland, Joint Quantum Institute, College Park, Maryland 20742, USA

³Institute for the Research in Electronics and Applied Physics, University of Maryland, College Park, Maryland 20742, USA

 (Received 8 December 2023; revised 12 June 2024; accepted 22 October 2024; published 6 December 2024)

Experimental advances in cavity QED are raising the prospect of using light to probe quantum materials beyond the linear response regime. The capability to access quantum coherent phenomena would significantly advance the field. However, theoretical work on many-body systems coupled to light in the quantum coherent regime has been select. Here, we investigate the radiative properties of a finite-sized quantum wire in a microwave cavity. Examples of quantum wires include single-walled carbon nanotubes, a key experimental system in the field of nano-optics and plasmonics. We find that, for a variety of excited states, the repeated emission of photons results in the generation of many-body quantum entanglement. This leads to an increase in the rate at which subsequent photons are emitted, an example of Dicke superradiance. On the other hand, Pauli blocking tends to reduce this effect. Bosonization, the description of the excitations of a one-dimensional electron system as a gas of bosons, is found to be a powerful theoretical tool in this context. Its application means that many of our results generalize to wires with strong electron-electron interactions. The quantum wire thus represents a new platform to realize Dicke-model physics that does not rely on the various fine tunings necessary in traditional realizations involving many spatially isolated emitters. More broadly, this work demonstrates how quantum entanglement can be generated and measured in a many-body system.

DOI: [10.1103/PRXQuantum.5.040338](https://doi.org/10.1103/PRXQuantum.5.040338)

I. INTRODUCTION

Light-matter coupling underlies many of the experimental probes of condensed-matter systems. In the linear-response regime, a system excited by an external perturbation relaxes before it can be excited again [1]. On the other hand, the observation of certain quantum coherent effects requires a probe to interact with a system many times before decoherence sets in. This places a lower limit on the probe-system coupling strength [2–5]. The inherent weakness of light-matter coupling—dictated by the fine structure constant $\alpha = 1/137$ —would seem to preclude accessing the quantum regime using light. However, strong light-matter coupling can be achieved using cavity QED technology [2–8].

The possibility of probing or even altering quantum systems using cavity QED is now receiving a great deal

of attention [2–18]. Low-dimensional quantum systems are particularly well suited to such approaches [7,10–12,17,19,20]. Plasmons, a fundamental excitation of one-dimensional (1D) electron liquids, have been observed in carbon nanotubes [21]. Recently, the spectrum of plasmons in graphene has been probed in a van der Waals heterostructure microcavity [22]. More ambitious proposals call for the use of light to fundamentally alter the properties of condensed-matter systems [2].

While much of this excitement has been stimulated by recent advances in cavity-QED technology [2], the study of light-coupled matter in the quantum coherent regime has a long history. The Dicke model, introduced nearly 70 years ago [23], describes N noninteracting spin-1/2 degrees of freedom coupled to a photonic mode [24–27]. A signal prediction of the model is superradiance, the phenomenon in which radiation generates entanglement, and this in turn leads to an increase in the rate that subsequent radiation is emitted [9,25].

In order to realize the full potential of recent technological advances to probe quantum materials, a greater understanding of condensed-matter systems in the quantum coherent regime is needed. This motivates the current work, which investigates a finite-sized quantum wire in a

*Contact author: victor.bradley@ttu.edu

Published by the American Physical Society under the terms of the [Creative Commons Attribution 4.0 International](https://creativecommons.org/licenses/by/4.0/) license. Further distribution of this work must maintain attribution to the author(s) and the published article's title, journal citation, and DOI.

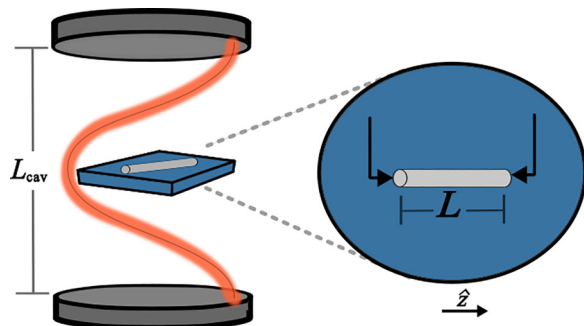


FIG. 1. A quantum wire in a microcavity coupled to a single photonic mode. Inset shows top-down view of the wire on a substrate. Leads, indicated by arrows, are attached at the ends of the wire.

microcavity. A sketch of the proposed setup is shown in Fig. 1. Our analysis focuses on specific excited states of the wire and the subsequent radiative cascade. We detail the many-body states the system passes through as the system emits photons. For the case of a single electron-hole pair, we find that the photon emission generates momentum-space entanglement [28] between the electron and hole, which in turn leads to Dicke-like superradiance. This increasing emission rate closely tracks the growth of the entanglement entropy of the wire. For the case of two excited electrons with similar energies, Pauli blocking comes into play and reduces the effects of superradiance.

The proposed experimental setup leverages recent advances in the experimental technology associated with the fabrication of devices in microcavities [6,22]. The current proposal also benefits from the technological capabilities involving gating and lead connection to a sample in a microcavity [29,30]. We consider a cavity in the microwave regime. The 10- μm -wire considered here is resonant with 160-GHz cavity mode. Other realizations involving optical frequencies are also possible. Remarkably, the experiment presented in Ref. [22] has demonstrated measurements of plasmons in the THz gap, thus dramatically increasing the range of wire sizes that can be used. The light-matter coupling strength g (Hz) ideal for probing quantum materials is of intermediate strength—it should exceed the intrinsic decay rate of excited states in the wire, but still be small compared with the cavity-mode frequency. The latter constraint ensures that the wire and cavity mode do not hybridize.

This work makes use of bosonization, a theoretical technique that describes an electron gas or liquid in terms of noninteracting bosons. These bosons represent a “good” basis for the description of light-matter coupling. Additionally, the unitary transformation linking the electronic and bosonic bases [31] suggests a procedure for preparing certain excited states of the wire. While we discuss the preparation of many of the excited states considered

here, their preparation is likely difficult, particularly in the bad cavity limit considered here. However, the preparation of these states is not necessary to observe the physics described here. Rather, the specific states considered here give insight into the generic features of the radiative behavior. For example, the case of a single electron-hole pair is particularly important since all excited states of an electron gas are composed of such pairs.

The paper is organized as follows. In Sec. II, we introduce the physical setup of interest: a quantum wire coupled to a photonic mode. In Sec. III, the bosonization technique is introduced. Section IV presents several examples of cascades. In Sec. V, the effects of the curvature of the electron dispersion as well as electron-electron interactions are discussed. Finally, in Sec. VI, we present our conclusions and outlook for future work.

II. PHYSICAL SETUP

The physical setup, shown in Fig. 1, consists of a quantum wire of finite length L in a photonic microcavity with characteristic length L_{cav} . The fabrication of quantum wires in semiconducting heterostructure is routine, and here we propose their incorporation into a microcavity [22]. In Appendix B, estimates of possible experimental parameters are given.

Given that the strength of electron-electron interactions in one-dimensional quantum wires formed from semiconductor heterostructures is highly tunable [32], we focus on the case that the electrons are noninteracting. The effect of interactions is discussed in Sec. V. For theoretical convenience, the wire’s electrons are taken to be spin polarized, with a dispersion given by $\varepsilon_k = \hbar^2 k^2 / 2m_e$, where k and m_e are the wave number and mass of the electron and \hbar is the reduced Planck’s constant. Low-energy excitations of the wire are described by the effective Hamiltonian

$$H_0 = \sum_{j=-\Lambda}^{\Lambda} \hbar\omega_j c_j^\dagger c_j, \quad (1)$$

where the operator c_j^\dagger creates an electron in the j th single-electron state, which has an energy $\hbar\omega_j$. The integer j indexes the single-particle states, as shown in Fig. 2(a). The zero of energy is set by the Fermi level: we take $j = 0$ to be the highest energy state that is occupied when the quantum wire is in its ground state $|G\rangle$. The effective theory has a linear dispersion $\omega_j = v_F j / L$, where v_F is the Fermi velocity [33]. Effects associated with curvature of the dispersion will be addressed in Sec. V. The integer Λ is a high-energy cutoff.

As detailed below, we focus on the case in which the wire emits photons into a single cavity mode of frequency $n\omega_1$. The cavity-wire coupling strength is g (Hz). The loss rate of all cavity modes is taken to be κ , which for theoretical convenience, is assumed to be in the bad-cavity limit

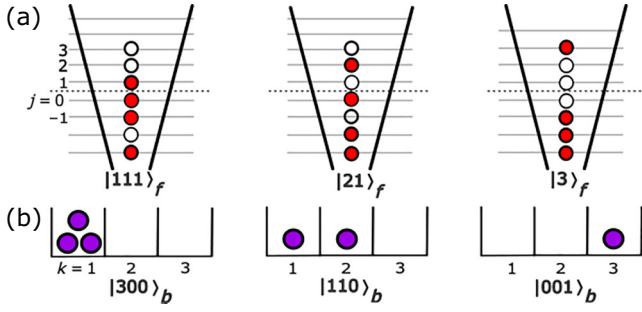


FIG. 2. Three excited states of the electron gas with energy $3\hbar\omega_1$ in the (a) electronic (fermionic) (b) bosonic bases. In (a), only the most energetic electrons are shown. These electronic and bosonic states are related by the unitary transformation Eq. (D6).

$g \ll \kappa$. In this regime, the characteristic rate at which the wire emits photons into the cavity is

$$\Omega = \frac{4g^2}{\kappa}, \quad (2)$$

as given by Fermi's golden rule, see Appendix A and Ref. [34]. Since $\Omega \ll \kappa$, this is also essentially the rate that photons are emitted into the bath coupled to the cavity mode.

It is important to consider other mechanisms that allow the quantum wire to relax. For example, electron-phonon scattering likely plays a role. Additionally, the wire can emit noncavity photons. The total rate of the various processes that do not result in the generation of a cavity photon is denoted by γ [6]. The cascades studied in this work require that $\gamma \ll \Omega$. Here, this condition defines the “quantum coherent regime” discussed in the Introduction. On the other hand, light-matter coupling should remain a weak perturbation with $\Omega \ll \omega_1$. This ensures that there is not strong hybridization of the quantum wire and the photonic mode.

We consider the radiative decay rate of the many-body state $|\alpha\rangle$, which we take to be an eigenstate of the Hamiltonian Eq. (1). Its decay rate is given by Fermi's golden rule [25]

$$\Gamma_\alpha = \Omega \langle \alpha | \mathcal{D}_n^\dagger \mathcal{D}_n | \alpha \rangle, \quad (3)$$

where

$$\mathcal{D}_n = \sum_m c_{m-n}^\dagger c_m. \quad (4)$$

Except for several examples discussed in Secs. IV C and V, we will consider the case $n = 1$. As described in Appendix A, the derivation of Eq. (3) assumes the dipole

approximation. The operator \mathcal{D}_n plays the role of a many-body lowering operator, taking $|\alpha\rangle$ to

$$|\alpha'\rangle = \frac{\mathcal{D}_n |\alpha\rangle}{\sqrt{\langle \alpha | \mathcal{D}_n^\dagger \mathcal{D}_n | \alpha \rangle}}, \quad (5)$$

its daughter state after the decay. The energy of the photon is $\hbar\omega_1$. Tacit to Eq. (5) is the assumption that the decay rate of an electron from state $j \rightarrow k$ depends on $j - k$, but is only weakly dependent on $j + k$. This assumption is discussed in Sec. V.

III. BOSONIZATION

The description of the electron gas in terms of electronic excitations can quickly become unwieldy because the operator \mathcal{D}_n tends to generate complicated superpositions. Fortunately, the bosonization technique offers an alternative basis [31] that is particularly useful in the present context. As we will see, it also can elucidate physics that is obscure in the electron basis. The bosonization technique provides a one-to-one mapping between the excitations of a 1D electron system and a gas of noninteracting bosons [31]. The Hamiltonian for these bosons is

$$H_B = \hbar\omega_1 \sum_{k=1}^{\infty} k b_k^\dagger b_k, \quad (6)$$

where b_k destroys a boson in the k th mode. This Hamiltonian describes an infinite number of harmonic oscillators with frequencies $\omega_1, 2\omega_1, 3\omega_1$, etc. The eigenstates of H_B are Fock states $|l_1 l_2 \dots\rangle_b$, where l_i is the occupation number of the i th bosonic mode. According to Eq. (6), the total energy of this state is $E = l_1 \hbar\omega_1 + l_2 (2\hbar\omega_1) + \dots$

To motivate this approach, consider the operator $\mathcal{D}_1^\dagger \mathcal{D}_1$ that appears in the expression for Γ_α in Eq. (3). We consider this operator in the subspace of the three excited states with energy $3\hbar\omega_1$. The degeneracy of this subspace is equal to the partitions of the integer 3, i.e., the number of distinct ways 3 can be written as a sum of integers: 3, 2 + 1, or 1 + 1 + 1 [31]. These partitions correspond to the states $|3\rangle_f$, $|21\rangle_f$, and $|111\rangle_f$, respectively, where $|\lambda_1 \lambda_2 \lambda_3 \dots\rangle_f$ is the excited state formed from the ground state by promoting the most energetic electron by an energy $\lambda_1 \hbar\omega_1$, the second-most energetic electron by $\lambda_2 \hbar\omega_1$, and so on (the subscript f indicates that this is the fermionic or electronic basis). Pauli exclusion requires that these integers satisfy $\lambda_1 \geq \lambda_2 \geq \lambda_3 \dots$. For instance, the state $|3\rangle_f = c_3^\dagger c_0 |G\rangle$. These three states are depicted in Fig. 2(a). The matrix elements of $\mathcal{D}_1^\dagger \mathcal{D}_1$ are

$$\mathcal{D}_1^\dagger \mathcal{D}_1 = \begin{pmatrix} 1 & 1 & 0 \\ 1 & 2 & 1 \\ 0 & 1 & 1 \end{pmatrix}, \quad (7)$$

in the basis that $|3\rangle_f$, $|21\rangle_f$, and $|111\rangle_f$ are represented by $(1\ 0\ 0)^T$, $(0\ 1\ 0)^T$, and $(0\ 0\ 1)^T$, respectively.

The eigenvalues of Eq. (7) are $\{3, 1, 0\}$. The significance of these numbers becomes apparent in the bosonic basis. Naturally, there are three bosonic states with energy $3\hbar\omega_1$, namely $|300\rangle_b = (b_1^\dagger)^3|G\rangle$, $|110\rangle_b = b_1^\dagger b_2^\dagger|G\rangle$, and $|001\rangle_b = b_3^\dagger|G\rangle$. Apparently, the eigenvalues 3, 1, and 0, correspond to the occupation number l_1 of these three states. The operator $\mathcal{D}_1^\dagger \mathcal{D}_1$ is thus diagonal in the bosonic basis. This is true in general and follows from the bosonization identity [31]

$$b_n = \frac{1}{\sqrt{n}} \mathcal{D}_n. \quad (8)$$

Thus, $\mathcal{D}_1^\dagger \mathcal{D}_1 = b_1^\dagger b_1$ is the number operator for the $k = 1$ mode. The unitary transformation linking the two bases diagonalizes $\mathcal{D}_1^\dagger \mathcal{D}_1$ (see Appendix D). For example, the third state shown in Fig. 2(a) is

$$|3\rangle_f = \frac{1}{\sqrt{6}}|300\rangle_b + \frac{1}{\sqrt{2}}|210\rangle_b + \frac{1}{\sqrt{3}}|001\rangle_b. \quad (9)$$

A general expression for the unitary transformation exists and is given by Eq. (D6) in Appendix D. It was first established in Ref. [31].

For the subspace with two units of energy, this transformation is straightforward to derive directly from the operator identity Eq. (8). For example, the expression

$$|01\rangle_b = \frac{1}{\sqrt{2}}(|2\rangle_f - |11\rangle_f) \quad (10)$$

can be obtained by acting the identity (8) for $n = 2$,

$$b_2^\dagger = \frac{1}{\sqrt{2}} \sum_m c_{m+2}^\dagger c_m, \quad (11)$$

on the ground state. Note that the minus sign in Eq. (10) is required by the anticommutation relations obeyed by fermionic operators [35]. It follows that

$$|20\rangle_b = \frac{1}{\sqrt{2}}(|2\rangle_f + |11\rangle_f), \quad (12)$$

since $|01\rangle_b$ and $|20\rangle_b$ are orthogonal.

Knowledge of the transformation between the bosonic and electron bases suggests a method for the preparation of a number of different initial states using measurement and postselection. While the application of this method is difficult in the bad-cavity limit, we briefly outline this preparation scheme since it could be of use in high- Q cavities. This method is based on the capability to measure

the occupation of a single-electron level j (the numbering scheme for these states is shown in Fig. 2). This can be done by measuring the conductance through a wire when the energy level is resonant with external leads. Due to Pauli blocking, an occupied level would prevent or suppress conductance through the wire. As an example, consider a quantum wire that has been excited by exactly two photons of energy $\hbar\omega_1$. It is thus in the state $|20\rangle_b$. Now, a conductance measurement reveals that the $j = 1$ level is occupied. According to Eq. (12), the wire would then be in the state $|11\rangle_f$. On the other hand, if this level is unoccupied, then the system will be in the state $|2\rangle_f$.

IV. CASCADES

This section presents our key results. We consider the sequence of many-body states of the wire as photons are emitted,

$$||1\rangle\rangle \xrightarrow{\Gamma_1} ||2\rangle\rangle \xrightarrow{\Gamma_2} \dots \xrightarrow{\Gamma_{N-1}} ||N\rangle\rangle, \quad (13)$$

where the double brace notation indicates that the state is being labeled according to the order it appears in the cascade. For example, $||1\rangle\rangle$ is the initial (electronic) state in the cascade, $||2\rangle\rangle$ is the second, and $||N\rangle\rangle$ is the last. The decay rate of the state $||m\rangle\rangle$ is denoted by Γ_m .

Except where stated, we will consider the case in which the wire is coupled to a cavity mode of frequency ω_1 . This corresponds to the case $n = 1$. In this case, the states in the cascade can be obtained by applying the operator \mathcal{D}_1 , or equivalently b_1 , to the initial state $||1\rangle\rangle$ repeatedly. The subsequent states and their decay rates are given by Eqs. (5) and (3), respectively. The cascade terminates with the state $||N\rangle\rangle$ that is annihilated by b_1 , i.e., $b_1||N\rangle\rangle = 0$. In certain cases, the bosonic basis is unwieldy and it is advantageous to work in the electronic basis.

A. Excited bosonic mode of wire

We consider an initial state consisting of N bosonic excitations in the $k = 1$ mode of the wire, i.e., $||1\rangle\rangle = |N, 000 \dots\rangle_b$. The intermediate states in the cascade, obtained by repeatedly applying b_1 to the initial state, are

$$||m\rangle\rangle = |N - m + 1, 000 \dots\rangle_b. \quad (14)$$

The decay rate of these states is given by Eq. (3),

$$\Gamma_m = \Omega(N - m + 1). \quad (15)$$

This result has a particularly simple interpretation: the rate reflects the fact that each bosonic excitation can decay independently and thus Γ_m is proportional to the number of bosons remaining in the $k = 1$ mode.

The creation of a pure number state using photons is challenging in the bad-cavity limit. On the other hand,

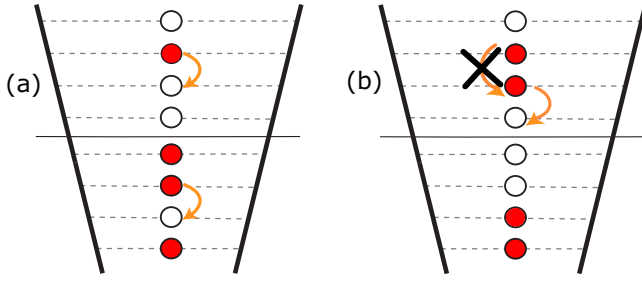


FIG. 3. (a) Transition $\|1\rangle\rangle \rightarrow \|2\rangle\rangle$ for the electron-hole pair, with $\|1\rangle\rangle = |3, 3\rangle_{\text{eh}}$ and $\|2\rangle\rangle = (|3, 2\rangle_{\text{eh}} + |2, 3\rangle_{\text{eh}})/\sqrt{2}$. (b) The decay of a two-electron state with $R = 1$. The decay of the more energetic electron is Pauli blocked, as indicated by the “X.”

a coherent state can be created by applying a classical drive in the presence of loss [34]. Similarly, driving the quantum wire with a classical electromagnetic field at a frequency $k\omega_1$ will generate an electronic coherent state of the form $e^{\alpha b_k^\dagger}|0\rangle$. The radiative properties of coherent states is treated using the quantum trajectories method in Ref. [36].

A simple but profound aspect emerges from this example: a 1D electron gas with a linear spectrum does not fluoresce: if the gas absorbs some number of photons of various energies, then it can only relax by emitting the exact same population of photons. Although this fact is not obvious in terms of the electrons, it is apparent in the bosonic basis. This feature is spoiled by the nonlinearity of the electron dispersion, as discussed in Sec. V.

B. Electron-hole pair

Any excited state of an electron gas is composed of electron-hole pairs. Here, we consider the cascade initiated by the creation of a single electron-hole pair: $\|1\rangle\rangle = |N_e, N_h\rangle_{\text{eh}}$, where $|i, j\rangle_{\text{eh}} = c_i^\dagger c_{-j+1}|G\rangle$ has an electron and hole in the single-particle levels i and $-j + 1$, respectively. The state $|3, 3\rangle_{\text{eh}}$ is depicted Fig. 3(a). (Initializing the system in this state is subtle and it cannot be generated by simply allowing the ground state to absorb a single photon of energy $5\hbar\omega_1$.) The final state in the cascade is the ground state $|G\rangle$.

For $m < N_e, N_h$, neither the electron nor the hole has reached the top of the Fermi sea at $j \sim 0$ where it would be Pauli blocked. In this case, the many-body wave function can be obtained by applying Eq. (5) repeatedly, which yields

$$\|m\rangle\rangle = \frac{1}{\sqrt{\mathcal{N}_m}} \sum_{k=0}^{m-1} \binom{m-1}{k} |N_e - k, N_h - m + k + 1\rangle_{\text{eh}}, \quad (16)$$

where

$$\mathcal{N}_m = \binom{2m-2}{m-1}. \quad (17)$$

For example,

$$\|3\rangle\rangle = \frac{1}{\sqrt{6}} (|N_e - 2, N_h\rangle_{\text{eh}} + 2|N_e - 1, N_h - 1\rangle_{\text{eh}} + |N_e, N_h - 2\rangle_{\text{eh}}) \quad (18)$$

is the third state in the cascade.

That $\|m\rangle\rangle$ is normalized follows from the combinatoric identity known as Vandermonde’s convolution [37]. From the relation

$$\mathcal{D}_1 \|m\rangle\rangle = \sqrt{\frac{\mathcal{N}_{m+1}}{\mathcal{N}_m}} \|m+1\rangle\rangle \quad (19)$$

and Eq. (3), we find that the rate at which the state $\|m\rangle\rangle$ decays is

$$\Gamma_m = \left(4 - \frac{2}{m}\right) \Omega. \quad (20)$$

The decay rate of a single electron or hole is Ω and so the initial rate 2Ω for $m = 1$ suggests that the electron and hole decay independently of each other. It is clear from the wave function Eq. (16) that photon emission generates entanglement between the electron and hole. This accounts for the increase in the rate Eq. (20), and represents an example of superradiance. For $1 \ll m < N_e, N_h$, the rate approaches $(1+1)^2\Omega = 4\Omega$, which corresponds to an emission process that is fully coherent since the quantum-mechanical amplitudes, rather than the rates, add.

C. Multiple electron-hole pairs

The generalization to multiple electron-hole pairs is straightforward. As long as none of the electrons or holes are Pauli blocked, either at the top of the Fermi sea or by each other, the many-body wave function is obtained by replacing the binomial coefficients that appear in Eq. (16) by the appropriate multinomial coefficients. For P electron-hole pairs, the initial decay rate is $2P\Omega$. The rate approaches $(2P)^2\Omega$ after many steps.

As mentioned above, the emission rate Eq. (20) is increasing in m due to the growing entanglement between the electron and hole. This is an example of momentum-space entanglement [28]. The entanglement entropy of the electron-hole pair is

$$S = - \sum_k p_k \ln p_k, \quad (21)$$

where $p_k = \binom{m-1}{k}^2 / \mathcal{N}_m$. As shown in Fig. 4, the entanglement entropy grows as the cascade proceeds. For large m , a

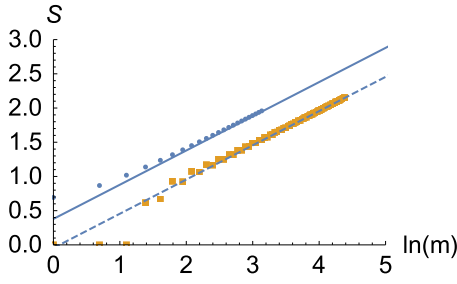


FIG. 4. Entanglement entropy between an electron and hole (circles) and two electrons (squares) versus $\ln m$. The solid and dotted lines indicate the asymptotic behavior of the entanglement entropy for these cases, respectively. The solid line is given by Eq. (22).

Gaussian approximation can be used to estimate p_k , which gives

$$S = \frac{1}{2} \ln m + c, \quad (22)$$

where $c = \ln(\sqrt{\pi}/2) + \frac{1}{2} \approx 0.38$. The entanglement entropy is a measure of the effective number of electron-hole pair states in the superposition Eq. (16). The factor of $1/2$ appearing in Eq. (22) is natural given that the wave function has a width \sqrt{m} in the large m limit.

For $m > N_e, N_h$, there is amplitude for the electron or the hole to reach the top of the Fermi sea and thus become Pauli blocked. At this point in the cascade, the wave function is no longer given by Eq. (16) and the decay rates will be less than those in Eq. (20). In Fig. 5, the rates Γ_m for the cascade $N_e = N_h = 4$ are shown. For $m \leq 3$, the rates conform to Eq. (20). For $m > 4$, the rates are decreasing in m as the system approaches the ground state.

We now consider a cascade that maps directly to the Dicke model. The initial state is formed by promoting each of the \bar{N} most energetic electrons in the ground state by an energy $\bar{N}\hbar\omega_1$, i.e., $\|1\rangle\rangle$ is $|\bar{N}\bar{N}\bar{N}\dots\rangle_f$. We then consider

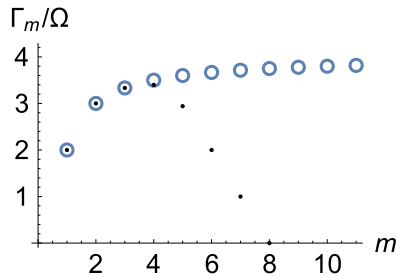


FIG. 5. The dimensionless decay rates Γ_m/Ω (black dots) of the states in the cascade with initial state $\|1\rangle\rangle = |4, 4\rangle_{\text{eh}}$, given by Eq. (3). For $m \leq 3$, the rate is consistent with Eq. (20) (open circles). Once $m > 3$, there is nonzero amplitude for the electron or hole to reach the Fermi surface and become Pauli blocked, and so the rate is suppressed.

the decay of this state via the emission of photons of energy $\bar{N}\hbar\omega_1$ for which $n = \bar{N}$. The final state is the ground state. In this case, we take the resonant cavity mode to have an energy $\bar{N}\hbar\omega_1$.

Due to the Pauli exclusion principle, each electron can only decay once and thus can be represented by a single Dicke spin ($1/2$). In order to demonstrate this correspondence, we will calculate the rates and states for $\bar{N} = 3$. Consider the initial state $\|1\rangle\rangle = |333\rangle_f$. Subsequent states in the cascade are found by repeatedly applying the lowering operator b_3 (in this example, transitions of energy $3\omega_1$ are considered). The state $|333\rangle_f$ can be expressed as a superposition of 12 bosonic basis states. The second state in the cascade is $\|2\rangle\rangle$, which is proportional to $b_3|333\rangle_f$, and takes the form

$$\begin{aligned} \|2\rangle\rangle = & -\frac{1}{2\sqrt{15}}|0\rangle_a + \frac{1}{2\sqrt{3}}|0\rangle_b - \frac{1}{\sqrt{6}}|0\rangle_d \\ & - \frac{1}{\sqrt{15}}|0\rangle_e + \sqrt{\frac{2}{3}}|2\rangle_0, \end{aligned} \quad (23)$$

where the state $|2\rangle_0$ has two quanta in the $m = 3$ mode while the other modes (not shown) are in their ground state. The states $|0\rangle_x$ with $x = a, b, d, e$ have 0 quanta in the $m = 3$ bosonic mode but have other modes that are excited. We find

$$\langle\langle 2 \| b_3 \| 1 \rangle\rangle = 1, \quad (24)$$

$$\langle\langle 3 \| b_3 \| 2 \rangle\rangle = \frac{2}{\sqrt{3}}, \quad (25)$$

$$\langle\langle 4 \| b_3 \| 3 \rangle\rangle = 1. \quad (26)$$

The decay rates Eq. (3) are proportional to the square of these amplitudes and follow the ratio 3 : 4 : 3.

These rates can be compared to those of the Dicke model with $\bar{N} = 3$ spins. The states in the Dicke model are characterized by the magnetic quantum number $M = J, J - 1, \dots, -J$, which is the z component of the total angular momentum $J = \bar{N}/2$ of the spins. The rate of decay of the state with magnetic quantum number M is [25]

$$\Gamma_M \propto (J + M)(J - M + 1). \quad (27)$$

These rates of decay also follow the ratio 3 : 4 : 3 for $J = \frac{3}{2}$ and $M = \frac{3}{2}, \frac{1}{2}, -\frac{1}{2}$.

We describe the preparation of the state $|333\rangle_f$ based on the scheme outlined in Sec. III. The wire, initially in its ground state, is excited by two $4\hbar\omega_1$ photons and one $1\hbar\omega_1$ photon. This results in the state $|1002\rangle_b$. Writing this state as a superposition of electronic states $|\dots\rangle_f$ shows that $|333\rangle_f$ can be obtained by measuring the conductance through the single-electron states $j = 2$ and $j = 3$. If both states are found to be occupied, then the measurement will

have collapsed the wave function to $|333\rangle_f$. This procedure is based on the unitary transformation connecting the bosonic and electron bases described in Appendix D.

D. Pair of electrons

We now consider a cascade in which two electrons are initially excited. This case is more complex than that of an electron-hole pair due to the fact that the lower-energy electron can Pauli block the higher-energy one. We consider two electrons far above a filled Fermi sea that are initially separated by R energy levels. This initial state is denoted $\|1\rangle\rangle = |N_e, N_e - R\rangle_{ee}$, where $N_e \gg R$ and the state $|j, k\rangle_{ee} = c_j^\dagger c_k^\dagger |G\rangle$ consists of electrons in the single-particle states j and k above a filled Fermi sea.

For $m < R$, there have not been a sufficient number of decays for the top electron to be Pauli blocked. Thus, the form of the wave function and the rates are the same as those of the electron and hole for $m < N$. However, once $m > R$, Pauli blocking comes into play, as illustrated in Fig. 3(b). The electronic wave function, valid in both of these cases, is given by

$$\|m\rangle\rangle = \frac{1}{\sqrt{\mathcal{N}'_m}} \sum_{k=0}^{m-1} \eta_k |N_e - k, N_e - R - m + k + 1\rangle_{ee}, \quad (28)$$

where

$$\eta_k = \left[\binom{m-1}{k} - \binom{m-1}{k-R} \right]_+, \quad (29)$$

and $[x]_+ = x$ for $x > 0$ and 0 otherwise. We use the convention that the second term in brackets is zero for $k < R$. The normalization constant \mathcal{N}'_m does not have a simple form. The first term in brackets is the same that appears in the wave function Eq. (16). The second term accounts for Pauli blocking. The quantity η_k appears in a closely related combinatorics problem: it is the number of possible paths in a ‘‘truncated’’ version of Pascal’s triangle, which has a vertical absorbing wall [38]. In that context, the first term in η_k is the total number of paths that arrive at a point, while the second is the number of paths that also hit the absorbing wall. In the present context, the latter correspond to those decays that violate Pauli exclusion.

We now consider the decay rate of the states $\|m\rangle\rangle$, which are denoted by Γ'_m . The effects of Pauli blocking are evident in the behavior of $\Gamma_m - \Gamma'_m$, where Γ_m is given by Eq. (20). We consider the case $N_e \gg 1$ and $R = 10$. As shown in Fig. 6, $\Gamma_m = \Gamma'_m$ for $m < R = 10$. For $m > R$, $\Gamma'_m < \Gamma_m$. The suppression of Γ'_m reflects the fact that the higher-energy electron must ‘‘wait’’ for the lower one to decay. Interestingly, the difference $\Gamma_m - \Gamma'_m$ exhibits non-monotonic behavior in m , peaking at $m \approx 50$. Figure 6 is suggestive of the fact that $\Gamma_m - \Gamma'_m$ tends to zero for m

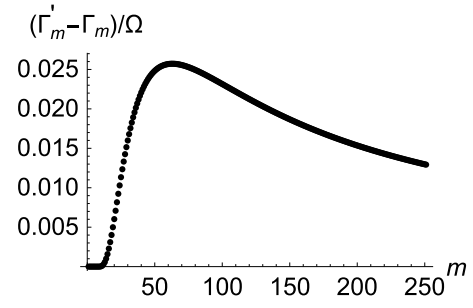


FIG. 6. The difference in decay rates $(\Gamma_m - \Gamma'_m)/\Omega$ for the cascades involving an electron-hole pair and two electrons.

large (but still $< N_e$). Below, we argue that this is indeed the case.

The entanglement entropy for the case of two electrons can be defined in a manner analogous to the case of an electron and hole. In Fig. 4, we have plotted the entanglement entropy between two electrons for $R = 1$. For small m , there is a conspicuous alternating pattern in the entanglement entropy S . This parity effect arises because of the form of \mathcal{D}_1 . In particular, if the state $\|m\rangle\rangle$ contains a Pauli-blocked electron, $\|m+1\rangle\rangle$ cannot. The asymptotic behavior of S for large m can be estimated from η_k using a Gaussian approximation for the binomial coefficients. We find that the entanglement entropy again takes the asymptotic form given by Eq. (22) where now $c \approx -0.045$. This constant is less than c for the electron-hole case, another consequence of Pauli blocking. In the large m limit, the Gaussian approximation gives $D_1 \|m\rangle\rangle \simeq 2 \|m\rangle\rangle$, with corrections that vanish as $m \rightarrow \infty$. Together with Eq. (3), this shows that $\Gamma'_m \rightarrow 4\Omega$. Since $\Gamma_m \rightarrow 4\Omega$ as well [Eq. (20)], we find that $\Gamma_m - \Gamma'_m$ indeed tends to zero for $m \rightarrow \infty$, as claimed above.

V. PHASE COHERENCE

Phase coherence is crucial for superradiance. Here, we discuss how phase coherence is maintained in the quantum wire. We also consider a mechanism for its loss. Phase coherence is protected in the quantum wire system in several ways. First, the operator \mathcal{D}_n remains coherent because of the linearity of the electron dispersion. This guarantees that every term in the sum \mathcal{D}_n has the same dynamical phase. Phase coherence is also maintained by the form of \mathcal{M}_{jk} . The matrix elements are functions of $j - k$ but depend only weakly on $j + k$ (see Appendix A). Thus, the phase coherence arises from the universal properties of the 1D electron gas. Unlike the original Dicke model [24], these features do not rely on the fine tuning.

There are a number of ways in which phase coherence can be lost. Here, we explore loss of coherence due to a massive dispersion ε_k . We replace the linear dispersion

given in Sec. II with

$$\omega_j = \frac{\pi v_F}{L} j + \frac{\pi^2 \hbar}{2m_e L^2} j^2, \quad (30)$$

which is obtained by expanding ε_k around the Fermi momentum k_F . Consider a cascade with the initial state $|1\rangle = |\Psi(t)\rangle = |20\rangle_b$. Its time dependence can be written as

$$|\Psi(t)\rangle = \frac{1}{\sqrt{2}} (|2\rangle_f + e^{i\Delta t} |11\rangle_f), \quad (31)$$

where the offset energy $\Delta = \omega_2 - 2\omega_1 \propto 1/m_e$ arises from the nonlinearity of the dispersion. Writing Eq. (31) in the bosonic basis, we have

$$|\Psi(t)\rangle = \frac{1}{2} [(1 + e^{i\Delta t}) |20\rangle_b + (1 - e^{i\Delta t}) |01\rangle_b]. \quad (32)$$

For decay rates $\Omega \gg \Delta$, the state $|\Psi(t)\rangle$ decays before it evolves significantly in time. In this regime, the decay rate is 2Ω , i.e., the same as $|20\rangle_b$. For $\Delta \gg \Omega$, the decay rate is Ω and, as expected, we find that the loss of phase coherence reduces the rate of photon emission. In the Dicke model, the loss of phase coherence leads to a many-body wave function with a mix of different total angular momenta J [25].

The above example shows that for a nonlinear dispersion, the bosonic states are no longer eigenstates of the electronic Hamiltonian. The significance of the linear dispersion is that it exhibits particle-hole symmetry. The particle-hole symmetry operator, which we denote by \mathcal{P} , interchanges electrons and holes (a formal definition is given in Appendix D). For example, consider the action of the particle-hole symmetry operator on the state formed by promoting the topmost electron in the ground state by $2\hbar\omega_1$, i.e., $\mathcal{P}|2\rangle_f$. The resultant state can be formed by *demoting* the bottom-most *hole* by the same energy, giving $|11\rangle_f$. Thus,

$$\mathcal{P}|2\rangle_f = |11\rangle_f. \quad (33)$$

Since $\mathcal{P}^2 = 1$, we also have that $\mathcal{P}|11\rangle_f = |2\rangle_f$. It then follows that $|20\rangle_b$, given by Eq. (12) is an eigenstate of \mathcal{P} with eigenvalue $+1$. This is not a coincidence—every bosonic basis state $|l_1 l_2 \dots\rangle_b$ is an eigenstate of \mathcal{P} with an eigenvalue $(-1)^{\ell_2 + \ell_4 + \dots}$, as explained in Appendix D. For a linear spectrum, the particle-hole operator \mathcal{P} commutes with the Hamiltonian and so the states $|20\rangle_b$ and $|01\rangle_b$ are guaranteed to be degenerate.

Another consequence of a massive dispersion is that it gives rise to fluorescence. The lack of fluorescence of a wire with a perfectly linear spectrum was discussed in Sec. IV. Consider the situation depicted in Fig. 7 in which an electron gas is initially prepared in the state $|001\rangle_b$

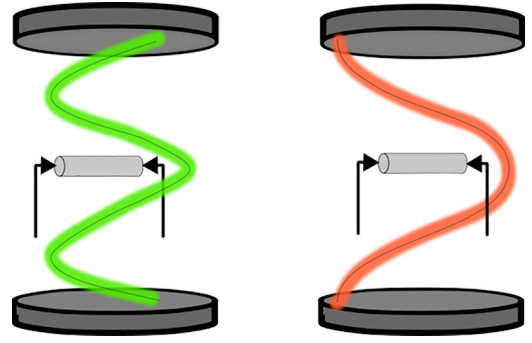


FIG. 7. Nontrivial fluorescence of an electron gas arising from a nonlinear single-electron dispersion. (left) The electron system is excited by the absorption of a $3\hbar\omega_1$ photon. After a time approximately $1/\Delta$, the system can decay by emitting a photon with energy $\hbar\omega_1$ (right).

through the absorption of a $3\hbar\omega_1$ photon. In this case, the system can decay by the emission of $\hbar\omega_1$ -energy photons, as we now argue. The state $|001\rangle_b$ can be expressed in terms of the electron basis states, which are now eigenstates [see Eq. (D7)]. After a time approximately $1/\Delta$, the wave function has significant overlap with the $|300\rangle_b$ state. The system can thus decay by emitting ω_1 photons.

We briefly remark that even for strong electron-electron interactions, the system's excitations can still be described by a gas of bosons [31]. This approach to handling interactions is known as the Luttinger liquid model. For strong interactions, there is no longer a simple transformation between the electron excitations and the bosons. While this complicates state preparation, the bosonic basis still accounts for the radiative properties of the liquid. The spectrum still consists of equally spaced energy levels, which is crucial to the phase coherence of the excited states. It is worth mentioning that certain interactions can give rise to anharmonic couplings between the bosons, but these couplings are weak [39].

VI. SUMMARY AND CONCLUSIONS

In this work, we investigated a quantum wire coupled to microwaves in a microcavity. Working in the quantum coherent regime, we found that this system exhibits Dicke-like superradiance. Phase coherence of the system is protected by the linearity of the low-energy spectrum. For generic initial states, the decay rates are controlled by superradiance and Pauli blocking. This work demonstrates how quantum entanglement can be both generated and measured in quantum wires. Bosonization was found to be a natural basis to describe light-matter coupling in a one-dimensional electron gas.

Here, we considered the case in which photons are emitted into only one mode of the microcavity. Furthermore, this mode was assumed to be sufficiently lossy so that the

so-called bad-cavity limit applied. While these assumptions simplified the analysis, state preparation is likely challenging in the bad-cavity limit. Given our understanding of the Dicke mode, it is natural to expect that the results presented here generalize to high- Q cavities for which the prospects for state preparation are more favorable. Generalizing this work to the high- Q regime represents an important area for future work.

We have found that the quantum wire in a microcavity is a platform to explore Dicke model physics. The proposed experiment offers several advantages over standard realizations, which typically involve a collection of spatially separated two-state systems coupled to the same electromagnetic mode. Such setups require the fine tuning of both the excitation energies of the resonators and their coupling strengths to the electromagnetic mode [24,27]. Here, neither type of fine tuning is required.

ACKNOWLEDGMENTS

The authors gratefully acknowledge productive conversations with Mike Stone and Smitha Vishveshwara. We also thank Myoung-Hwan Kim and Zachary Brown for their insightful comments.

APPENDIX A: MANY-BODY DIPOLE OPERATOR AND SINGLE-PARTICLE WAVE FUNCTIONS

According to Fermi's golden rule, the rate of decay of the state $|\alpha\rangle$ to the state $|\beta\rangle$ through the emission of a photon of energy $\hbar\omega_n$ is given by [34]

$$\Gamma_{\alpha\beta} = \frac{2\omega_n}{\varepsilon_0\hbar V_0\kappa} |\langle\beta|\wp|\alpha\rangle|^2 U_n(\mathbf{x}_0)^2, \quad (\text{A1})$$

in the dipole approximation. The dipole operator is $\wp = e \int dz z c_z^\dagger c_z$, where c_z annihilates an electron at z and e is the electron charge. The mode function $U_n(\mathbf{x}_0)$, evaluated at the wire's position \mathbf{x}_0 , accounts for the spatial variation of the n th cavity mode [40]. The states $|\alpha\rangle$ and $|\beta\rangle$ are eigenstates of the Hamiltonian and differ by an energy $\hbar\omega_n$. Here, ε_0 permittivity of free space, V_0 is the modal volume of the microcavity, and κ is its photon decay rate. The operator c_z can be written as $c_z = \sum_j \int dz \psi_j(z) c_j$, where $\psi_j(z)$ is the single-particle functions for the j th single-electron state. Substituting this mode expansion into the expression for the dipole operator gives $\wp = \sum_{jk} \mathcal{M}_{j-k} c_j^\dagger c_k$, where

$$\mathcal{M}_{j-k} = e \int_{-L/2}^{L/2} dz \psi_j^*(z) \psi_k(z) z. \quad (\text{A2})$$

The amplitudes \mathcal{M}_{j-k} are simply the dipole matrix elements between the first-quantized wave functions. This definition anticipates the fact that these matrix elements will only depend on the difference $j - k$.

The quantum wire, shown in Fig. 1, lies along the z axis with $-L/2 \leq z \leq L/2$. Here, we take particle-in-a-box boundary conditions $\psi_j(\pm L/2) = 0$, and let the number of electrons in the wire \mathcal{N} be even. The single-electron wave functions in this case are

$$\psi_j(z) = \begin{cases} \sqrt{\frac{2}{L}} \sin\left(\frac{\pi(j + \mathcal{N})z}{L}\right) & \text{for } j \text{ even,} \\ \sqrt{\frac{2}{L}} \cos\left(\frac{\pi(j + \mathcal{N})z}{L}\right) & \text{for } j \text{ odd.} \end{cases} \quad (\text{A3})$$

For states j and k with the same parity, i.e., for $j - k$ even, \mathcal{M}_{j-k} vanishes. For states with opposite parity, we have

$$\mathcal{M}_{j-k} = \frac{2eL}{\pi^2(j-k)^2} \quad (\text{A4})$$

for $\mathcal{N} \gg 1$ and $j, k \ll \mathcal{N}$. Corrections go as approximately $1/\mathcal{N}$.

We are interested in the total rate of decay Γ_α of the state $|\alpha\rangle$, which is given by the sum $\sum'_\beta \Gamma_{\alpha\beta}$ for which energy is conserved (the prime indicates this constraint). Using the form of \wp and the operator \mathcal{D}_n defined in Eq. (4), we have

$$\sum'_\beta |\langle\beta|\wp|\alpha\rangle|^2 = |\mathcal{M}_n|^2 \sum'_\beta |\langle\alpha|(\mathcal{D}_n + \mathcal{D}_n^\dagger)|\beta\rangle|^2 \quad (\text{A5})$$

$$= |\mathcal{M}_n|^2 \sum'_\beta \langle\alpha|\mathcal{D}_n^\dagger|\beta\rangle \langle\beta|\mathcal{D}_n|\alpha\rangle, \quad (\text{A6})$$

$$= |\mathcal{M}_n|^2 \langle\alpha|\mathcal{D}_n^\dagger \mathcal{D}_n|\alpha\rangle. \quad (\text{A7})$$

In going from Eqs. (A5) to (A6), we have dropped the constraint on $|\beta\rangle$ because energy conservation is automatically enforced by \mathcal{D}_n . Then, we use the fact that the unrestricted sum $\sum_\beta |\beta\rangle \langle\beta|$ is the identity. We thus obtain Eq. (3), where

$$g = \frac{\sqrt{2}eL}{\pi^2 n} \sqrt{\frac{\omega_n}{\varepsilon_0 \hbar V_0}} U_n(\mathbf{x}_0). \quad (\text{A8})$$

The expression for Γ_α generalizes the result given in Ref. [25] to the case of the 1D Fermi gas.

APPENDIX B: EXPERIMENTAL PARAMETERS

The fundamental excitation frequency of the electron gas is $\omega_1 = \pi v_F/L$. For quantum wires in semiconductors, the Fermi velocity $v_F \approx 10^5$ m/sec [32], and an order of magnitude larger in graphene-based structures [41]. There is considerable latitude in the selection of the wire's length, which sets ω_1 , the frequency of the fundamental excitation in the wire. For example, consider a quantum wire of length $L = 10$ μm , which gives $\omega_1 \approx 160$ GHz. This corresponds to a temperature of order 1 K, and thus the

experiment should be done in the range of hundreds of mK. The electron density can be controlled by the gate. For $\mathcal{N} \approx 4300$ electrons, we find that a lateral distance of 10 nm is sufficient to guarantee that no additional sidebands of the wire are occupied. These values correspond to a Fermi energy of 28 meV.

The quantum wire is to be fabricated from a semi-conducting heterostructure in a microcavity. We take the dimensions of the microcavity to be $2L \times 2L \times cL/v_F$. Equation (A8) gives a light-matter coupling of $g \approx 6$ GHz. For $\kappa \approx 60$ GHz, we have $\Omega \approx 2$ GHz from Eq. (2). In order for the constraints discussed below Eq. (2) to be satisfied, we require an internal decay rate of the wire $\gamma \lesssim 200$ MHz.

APPENDIX C: REPRESENTATION THEORY OF S_N

The symmetric group S_N is the group of permutations of N objects [42]. The order of S_N is the number of ways of arranging N distinguishable objects, i.e., $N!$. For example, $|S_3| = 6$. The elements of S_3 include the identity, denoted by $(1)(2)(3)$. This is the trivial permutation, which leaves the order of objects unchanged. Three elements of the group involve swapping two objects: $(12)(3)$, $(13)(2)$, and $(1)(23)$. The cycle notation $(12)(3)$ indicates the swapping of the first and second objects. Finally, there are two 3-cycles: (123) and (321) .

The elements of a group can be partitioned into sets known as conjugacy classes. A conjugacy class contains group elements of the same ‘‘type.’’ For example, the elements $(12)(3)$, $(13)(2)$, and $(1)(23)$, which swap exactly two elements, comprise one conjugacy class. For S_N , each conjugacy class contains those elements with the same cycle structure.

A representation of S_N is a set of elements obeying the group algebra. Of particular interest are the so-called irreducible matrix representations, which are the most efficient encoding of the group algebra using matrices [43]. Remarkably, there is a one-to-one correspondence between the irreducible representations of a group and its conjugacy classes. A key tool in representation theory is the character table. This table gives the trace of matrices representing the various group elements. As will be seen in Appendix D, the character table of S_N is related to the unitary transformation between the fermionic and bosonic bases for the 1D electron gas.

TABLE I. Character table of the symmetric group S_2 .



	(2, 0)	(0, 1)
	1	1
	1	-1

TABLE II. Character table of the symmetric group S_3 .

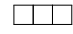
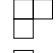
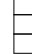
	(3, 0, 0)	(1, 1, 0)	(0, 0, 1)
	1	1	1
	2	0	-1
	1	-1	1

Table I is the character table for the group S_2 . Each column of a character table corresponds to a conjugacy class of the group. For S_N , these conjugacy classes are specified by the number of cycles of a given length. For example, the first column corresponding to the conjugacy class $(2, 0)$ contains the elements with two 1-cycles. There is only one group element in this class, namely the identity $(1)(2)$. The conjugacy class $(0, 1)$ contains the element with one 2-cycle, i.e., (12) .

Each row of a character table corresponds to an irreducible representation (irrep) of the group. These irreps can be represented by Young diagrams, which consist of N boxes. The various shapes represent these irreps [43]. In the trivial representation, each group element is represented by the number 1. This mapping trivially satisfies the group algebra. The second row in Table I corresponds to the alternating representation in which each group element is represented by the sign of the corresponding permutation, either ± 1 . In general, the first column of a character table gives the dimension of the irrep, i.e., the size of the matrices. This is because the first column corresponds to the identity element, and the trace of the identity matrix is equal to its dimension.

The group S_2 contains only one-dimensional representations. This stems from the fact that S_2 is Abelian. All non-Abelian groups necessarily contain at least one representation with a dimension >1 since simple numbers always commute. The group S_3 is non-Abelian and has a character table given in Table II. Note that the second irrep has a dimension of 2.

APPENDIX D: EXPLICIT MAPPING FROM FERMIONIC TO BOSONIC BASES

The unitary transformation between the fermionic and bosonic bases is, up to normalization factors, given by the characters of the symmetric group. As discussed in Appendix C, the rows and columns of a character table correspond to the irreps and conjugacy classes of a group, respectively.

There is a one-to-one correspondence between the conjugacy class (l_1, l_2, l_3, \dots) of S_N and the bosonic basis states $|l_1 l_2 \dots\rangle_b$, where $N = 1l_1 + 2l_2 + \dots$. Similarly, there is a one-to-one correspondence between the irreps of S_N and the electron basis states $|\lambda_1 \lambda_2 \lambda_3 \dots\rangle_f$, where the integers $\lambda_1 \geq \lambda_2 \geq \lambda_3 \dots \geq 0$ sum to N . As stated in the main

text, the state $|\lambda_1\lambda_2\lambda_3\cdots\rangle_f$ is created by promoting the most energetic electron by $\lambda_1\hbar\omega_1$ units of energy, the next most energetic electron by $\lambda_2\hbar\omega_2$ units of energy.

$$|\lambda_1\lambda_2\cdots\rangle_f = \cdots c_{\lambda_1-1}^\dagger c_{-1}^\dagger c_{\lambda_1}^\dagger c_0 |G\rangle. \quad (\text{D1})$$

Specifying this order is crucial in tracking signs associated with electron exchange.

As discussed in Appendix C, the irreps can be represented by Young diagrams. Thus, the Young diagrams can also represent electron states. The i th row of the Young diagram contains λ_i boxes. For example, the diagram



is a representation of the state $|3\rangle_f$, while the state $|111\rangle_f$ is represented by



The requirement that the series $\lambda_1, \lambda_2, \dots$ is not increasing enforces the Pauli exclusion principle. This imposes the rule that no row of a Young diagram can have more boxes than the row above it.

The transformation from the bosonic basis to the fermionic one is given by

$$|\lambda_1\lambda_2\lambda_3\cdots\rangle_f = \sum_C \frac{1}{\sqrt{m_C}} \chi_C^R |l_1 l_2 \cdots\rangle_b, \quad (\text{D2})$$

where χ_C^R is the character corresponding to irrep R of conjugacy class C and

$$m_C = 1^{l_1} 2^{l_2} \cdots l_1! l_2! \cdots l_n!. \quad (\text{D3})$$

The integer $N!/m_C$ is the number of group elements in the conjugacy class C . The fact that Eq. (D2) defines a unitary transformation follows directly from the orthogonality theorem of finite group representation theory [43].

We consider several special cases of this general expression. For the case of two excitations, the unitary transformation may be read from Eqs. (10) and (12),

$$U = \frac{1}{\sqrt{2}} \begin{pmatrix} 1 & 1 \\ 1 & -1 \end{pmatrix}. \quad (\text{D4})$$

This is consistent with Eq. (D2) and the character table for S_2 shown in Table I.

As a second example, consider the $\mathcal{D}_1^\dagger \mathcal{D}_1$ in the $3\hbar\omega_1$ subspace, as discussed in Sec. III of the main text. The

matrix given by Eq. (7) is diagonalized

$$U^\dagger (\mathcal{D}_1^\dagger \mathcal{D}_1) U = \begin{pmatrix} 3 & 0 & 0 \\ 0 & 1 & 0 \\ 0 & 0 & 0 \end{pmatrix}, \quad (\text{D5})$$

where the unitary matrix

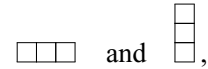
$$U = \frac{1}{\sqrt{6}} \begin{pmatrix} 1 & \sqrt{3} & \sqrt{2} \\ 2 & 0 & -\sqrt{2} \\ 1 & -\sqrt{3} & \sqrt{2} \end{pmatrix}. \quad (\text{D6})$$

This unitary matrix converts the bosonic basis states $|300\rangle_b, |110\rangle_b, |001\rangle_b$ to the electron basis states $|3\rangle_f, |21\rangle_f, |111\rangle_f$. Note that the pattern of signs in U matches those found in Table II. This is a special case of the transformation that appears on the right-hand side of Eq. (D2). The coefficients in Eq. (9) for $|3\rangle_f$ are given by the first row of U . The inverse transformation is given by U^\dagger since U is unitary. For example,

$$|001\rangle_b = \frac{1}{\sqrt{3}} |3\rangle_f - \frac{1}{\sqrt{3}} |21\rangle_f + \frac{1}{\sqrt{3}} |111\rangle_f. \quad (\text{D7})$$

These coefficients are given by the last column of U .

We briefly discuss the particle-hole symmetry operator \mathcal{P} . As discussed above, each fermionic state is represented by a Young diagram. The action of the particle-hole operator is to reflect this Young diagram along its main diagonal. The resultant diagram is said to be the conjugate of the first. For example, the diagrams corresponding to the states $|3\rangle_f$ and $|111\rangle_f$,



respectively, are conjugate to one another. Thus, the two corresponding fermionic states are particle-hole conjugates of each other and thus cannot be eigenstates of \mathcal{P} . But it is clear then that the state $(|3\rangle_f - |111\rangle_f)/\sqrt{2}$, which is the bosonic basis state $|110\rangle_b$, is an eigenstate of \mathcal{P} with eigenvalue -1 .

The action of the operator \mathcal{P} on an electron destruction operator for the i th energy level is

$$\mathcal{P} c_i \mathcal{P}^{-1} = (-1)^i c_{1-i}^\dagger. \quad (\text{D8})$$

This definition of particle-hole symmetry differs from the standard many-body definition taken in Ref. [44], for example. There, \mathcal{P} is antiunitary, $\mathcal{P}^2 = -1$. The fact that the action of \mathcal{P} is to take an operator at $i \rightarrow 1-i$ follows from the indexing of the single energy levels (see Fig. 2). The factor of $(-1)^i$ is required in order for the action of \mathcal{P} described above to be consistent with the sign choice made

in our definition of the fermionic basis states. For a bosonic operator b_n , we have

$$\mathcal{P}b_n\mathcal{P}^{-1} = (-1)^{n+1}b_n. \quad (\text{D9})$$

From this, it follows that the eigenvalue of \mathcal{P} of a bosonic state is controlled by the parity of the number of bosons in modes with even n ,

$$\mathcal{P}|\ell_1\ell_2\ell_3\cdots\rangle_b = (-1)^{\sum_i \ell_{2i}}|\ell_1\ell_2\ell_3\cdots\rangle_b. \quad (\text{D10})$$

The eigenvalue of \mathcal{P} is the sign of the permutations in the corresponding conjugacy class. This result is consistent with the fact that the number of even-numbered cycles in a permutation controls its sign.

-
- [1] G. W. F. Drake, *Springer Handbook of Atomic, Molecular, and Optical Physics* (Springer, Cham, 2006).
- [2] J. Bloch, A. Cavalleri, V. Galitski, M. Hafezi, and A. Rubio, Strongly correlated electron–photon systems, *Nature* **606**, 41 (2022).
- [3] N. Rivera and I. Kaminer, Light–matter interactions with photonic quasiparticles, *Nat. Rev. Phys.* **2**, 538 (2020).
- [4] K. Roux, H. Konishi, V. Helson, and J.-P. Brantut, Strongly correlated fermions strongly coupled to light, *Nat. Commun.* **11**, 2974 (2020).
- [5] A. Frisk Kockum, A. Miranowicz, S. De Liberato, S. Savasta, and F. Nori, Ultrastrong coupling between light and matter, *Nat. Rev. Phys.* **1**, 19 (2019).
- [6] F. Schlawin, D. M. Kennes, and M. A. Sentef, Cavity quantum materials, *Appl. Phys. Rev.* **9**, 011312 (2022).
- [7] A. Vasanelli, Y. Todorov, and C. Sirtori, Ultra-strong light–matter coupling and superradiance using dense electron gases, *C. R. Phys.* **17**, 861 (2016).
- [8] K. Kroeger, N. Dogra, R. Rosa-Medina, M. Paluch, F. Ferri, T. Donner, and T. Esslinger, Continuous feedback on a quantum gas coupled to an optical cavity, *New J. Phys.* **22**, 033020 (2020).
- [9] G. Baskaran, Superradiant superconductivity, *ArXiv:1211.4567*.
- [10] C. J. Eckhardt, G. Passetti, M. Othman, C. Karrasch, F. Cavaliere, M. A. Sentef, and D. M. Kennes, Quantum Floquet engineering with an exactly solvable tight-binding chain in a cavity, *Commun. Phys.* **5**, 1 (2022).
- [11] V. Rokaj, M. Ruggenthaler, F. G. Eich, and A. Rubio, Free electron gas in cavity quantum electrodynamics, *Phys. Rev. Res.* **4**, 013012 (2022).
- [12] P. Manasi and D. Roy, Light propagation through one-dimensional interacting open quantum systems, *Phys. Rev. A* **98**, 023802 (2018).
- [13] X. Yang, C. Vaswani, C. Sundahl, M. Mootz, L. Luo, J. H. Kang, I. E. Perakis, C. B. Eom, and J. Wang, Lightwave-driven gapless superconductivity and forbidden quantum beats by terahertz symmetry breaking, *Nat. Photonics* **13**, 707 (2019).
- [14] M. Mootz, L. Luo, J. Wang, and L. E. Perakis, Visualization and quantum control of light-accelerated condensates by terahertz multi-dimensional coherent spectroscopy, *Commun. Phys.* **5**, 47 (2022).
- [15] V. M. Kovalev and I. G. Savenko, Proposal for plasmon spectroscopy of fluctuations in low-dimensional superconductors, *Phys. Rev. Lett.* **124**, 207002 (2020).
- [16] L. Luo, M. Mootz, J. H. Kang, C. Huang, K. Eom, J. W. Lee, C. Vaswani, Y. G. Collantes, E. E. Hellstrom, I. E. Perakis, C. B. Eom, and J. Wang, Quantum coherence tomography of light-controlled superconductivity, *Nat. Phys.* **19**, 201 (2023).
- [17] F. Mivehvar, F. Piazza, T. Donner, and H. Ritsch, Cavity QED with quantum gases: New paradigms in many-body physics, *Adv. Phys.* **70**, 1 (2021).
- [18] K. Baumann, C. Guerlin, F. Brennecke, and T. Esslinger, Dicke quantum phase transition with a superfluid gas in an optical cavity, *Nature* **464**, 1301 (2010).
- [19] V. A. Pivovarov, A. S. Sheremet, L. V. Gerasimov, J. Laurat, and D. V. Kupriyanov, Quantum interface between light and a one-dimensional atomic system, *Phys. Rev. A* **101**, 053858 (2020).
- [20] D. Y. Joh, J. Kinder, L. H. Herman, S.-Y. Ju, M. A. Segal, J. N. Johnson, G. K.-L. Chan, and J. Park, Single-walled carbon nanotubes as excitonic optical wires, *Nat. Nanotechnol.* **6**, 51 (2011).
- [21] Z. Shi, X. Hong, H. A. Bechtel, B. Zeng, M. C. Martin, K. Watanabe, T. Taniguchi, Y.-R. Shen, and F. Wang, Observation of a Luttinger-liquid plasmon in metallic single-walled carbon nanotubes, *Nat. Photonics* **9**, 515 (2015).
- [22] G. Kipp, *et al.*, Cavity electrodynamics of van der Waals heterostructures, *ArXiv:2403.19745*.
- [23] R. H. Dicke, Coherence in spontaneous radiation processes, *Phys. Rev.* **93**, 99 (1954).
- [24] B. M. Garraway, The Dicke model in quantum optics: Dicke model revisited, *Philos. Trans. R. Soc. A* **369**, 1137 (2011).
- [25] M. Gross and S. Haroche, Superradiance: An essay on the theory of collective spontaneous emission, *Phys. Rep.* **93**, 301 (1982).
- [26] G. Vertogen and A. S. De Vries, The Dicke maser model, *Phys. Lett. A* **48**, 451 (1974).
- [27] P. Kirton, M. M. Roses, J. Keeling, and E. G. D. Torre, Introduction to the Dicke model: From equilibrium to nonequilibrium, and vice versa, *Adv. Quantum Technol.* **2**, 1800043 (2019).
- [28] M. O. Flynn, L.-H. Tang, A. Chandran, and C. R. Laumann, Momentum space entanglement of interacting fermions, *Phys. Rev. B* **107**, L081109 (2023).
- [29] D. Thureja, A. Imamoglu, T. Smoleński, I. Amelio, A. Popert, T. Chervy, X. Lu, S. Liu, K. Barmak, K. Watanabe, T. Taniguchi, D. J. Norris, M. Kroner, and P. A. Murthy, Electrically tunable quantum confinement of neutral excitons, *Nature* **606**, 298 (2022).
- [30] D. G. Suárez-Forero, R. Ni, S. Sarkar, M. J. Mehrabad, E. Mechtel, V. Simonyan, A. Grankin, K. Watanabe, T. Taniguchi, S. Park, H. Jang, M. Hafezi, and Y. Zhou, Chiral optical nano-cavity with atomically thin mirrors, *ArXiv:2308.04574*.
- [31] M. Stone, *Bosonization* (World Scientific, Singapore, 1994).

- [32] Y. Sato, S. Matsuo, C.-H. Hsu, P. Stano, K. Ueda, Y. Takeshige, H. Kamata, J. S. Lee, B. Shojaei, K. Wickramasinghe, J. Shabani, C. Palmström, Y. Tokura, D. Loss, and S. Tarucha, Strong electron-electron interactions of a Tomonaga-Luttinger liquid observed in InAs quantum wires, *Phys. Rev. B* **99**, 155304 (2019).
- [33] T. Giamarchi, *Quantum Physics in One Dimension* (Clarendon Press, Oxford, 2004), 1st ed.
- [34] M. O. Scully and M. S. Zubairy, *Quantum Optics* (Cambridge, Cambridge, 1997).
- [35] A. L. Fetter and J. D. Walecka, *Quantum Theory of Many-Particle Systems* (Dover Publications, Mineola, NY, 2003).
- [36] C. W. Gardiner and D. P. Zoller, *The Quantum World of Ultra-Cold Atoms and Light Book II* (Imperial College Press, London, 2015).
- [37] R. L. Graham, D. E. Knuth, and O. Patashnik, *Concrete Mathematics: A Foundation for Computer Science* (Addison-Wesley, Boston, Mass, 1994), 2nd ed.
- [38] R. G. Donnelly, M. W. Dunkum, C. George, and S. Schnake, Counting odd numbers in truncations of Pascal's triangle, [ArXiv:1807.08181](https://arxiv.org/abs/1807.08181).
- [39] W. DeGottardi, M. J. Gullans, S. Hegde, S. Vishveshwara, and M. Hafezi, Thermal radiation as a probe of one-dimensional electron liquids, *Phys. Rev. B* **99**, 235124 (2019).
- [40] D. F. Walls and G. J. Milburn, *Quantum Optics* (Springer Science & Business Media, Berlin, 2008).
- [41] C. Kane, L. Balents, and M. Fisher, Coulomb interactions and mesoscopic effects in carbon nanotubes, *Phys. Rev. Lett.* **79**, 5086 (1997).
- [42] A. Papantonopoulou, *Algebra: Pure & Applied* (Prentice Hall, London, 2002).
- [43] H. Georgi, *Lie Algebras in Particle Physics: From Isospin to Unified Theories* (Westview Press, Boulder, 1999).
- [44] C.-K. Chiu, J. C. Teo, A. P. Schnyder, and S. Ryu, Classification of topological quantum matter with symmetries, *Rev. Mod. Phys.* **88**, 035005 (2016).